# 9

### **Research Article**

Kun Liang, Lei Jin, Xuyan Deng, Ping Jiang and Li Yu\*

# Fine-tuning biexcitons-plasmon coherent states in a single nanocavity

https://doi.org/10.1515/nanoph-2023-0304 Received May 19, 2023; accepted July 10, 2023; published online July 25, 2023

**Abstract:** A tunable plexcitonic material that sustains multimode hybridization is highly desirable, which is vital for advanced quantum devices. However, the research about regulations of biexcitons-plasmon coherent states has rarely been reported. Here we apply single-nanoparticle scattering spectroscopy correlative with SEM imaging to identify biexcitons-plasmon interaction in a metal-semiconductor hybrid structure composed of a single Au@Ag nanoparticle, J-aggregates molecules and tungsten disulfide (WS2) monolayer. The mode competition within the localized plasmonic hotspots (~240 nm<sup>3</sup>) is revealed by continuously regulating the J-aggregates spacer. Two distinct anticrossings are observed at both excitons resonances, and large double Rabi splittings (137 meV and 124 meV) are obtained successfully. We establish experimentally that J-aggregates and WS<sub>2</sub> monolayer are responsible for the middle polariton states, while plasmon rarely contributes. Further calculations show that plasmonic nanocavity enables coherent energy exchange with different excitons by providing a highly enhanced localized E-field. In addition, we find that the multimode coupling strengths can be efficiently tuned by changing the cavity morphology and environment temperature, where the tuning spectral accuracy can reach up to 1 nm. Our findings uncover the distinctive properties of biexcitons-plasmon polaritons, suggest an easily obtainable multiqubit states platform, and open up a new way to construct nanoscale photonic devices.

\*Corresponding author: Li Yu, State Key Laboratory of Information Photonics and Optical Communications, School of Science, Beijing University of Posts and Telecommunications, Beijing, China,

E-mail: yuliyuli@bupt.edu.cn

**Kun Liang**, School of Electronic Engineering, Beijing University of Posts and Telecommunications, Beijing, China, E-mail: kunliang@bupt.edu.cn. https://orcid.org/0000-0002-5131-7361

**Lei Jin and Xuyan Deng**, School of Science, Beijing University of Posts and Telecommunications, Beijing, China

**Ping Jiang**, School of Science Microelectronics and Data Science, Anhui University of Technology, Maanshan, China

**Keywords:** biexcitons-plasmon coupling; double Rabi splitting; dynamic control; nano-optics; two-dimensional material

### 1 Introduction

Room-temperature strong coupling between quantum emitters (QEs) and plasmon polaritons has raised much attention in the optics and quantum physics communities, since it reveals a plethora of intriguing phenomena such as vacuum Rabi splitting [1, 2], Bose-Einstein condensation [3, 4], optical Stark effect [5, 6], entanglement [7, 8], and quantum network [9, 10]. It differs from weak coupling [11], where only the spontaneous emission rate was modified. Strong coupling [12] generates mixed states which possess both photonic and excitonic characters. The coherent energy transfer rate in the strong coupling regime surpasses the dissipation and decoherence rates. With the flourishing of nanofabrication technology and quantum electrodynamics, strong coupling systems exhibit great potential in many powerful applications, such as quantum light source [13, 14], ultrafast optical switching [15], superfluidity [16], single-molecule sensing [17], and quantum computing [18]. Up to now, a variety of plasmonic nanostructures have been proposed to minimize the mode volumes  $V_{\rm eff}$  since the coupling strength g is inversely proportional to  $\sqrt{V_{\rm eff}}$  [19]. Recently, even ultrasmall  $V_{\rm eff}$  below 1 nm<sup>3</sup> has been realized in the nanoparticle-on-mirror system [20]. The plasmonexciton strong coupled system has been successfully demonstrated at the single emitter level [21-24], building a firm foundation for functional quantum plasmonic devices. At the single nanocavity level, strong coupling between plasmon modes and 2D materials such as WS<sub>2</sub> [25, 26] and WSe<sub>2</sub> [27, 28] monolayer has been demonstrated, providing novel routes for active and plasmonics applications.

Despite these remarkable developments, the existing researches mainly focus on hybrid systems consisting of cavities and homogeneous quantum emitters, which only generate two coherent states. Considering the profound quantum effects and technological frontiers in the

multi-mode coupled systems [29-35] (e.g., quantum network, quantum computing, and nanolasers), strong coupling among three excitations is highly desirable. However, few have been reported in the single QEs-plasmonic nanocavity system due to the large Ohmic loss of metal [36]. One major challenge has to be overcome to trigger biexciton-plasmon strong coupling: The local electric field at heterogeneous QEs locations must be sufficiently enhanced to simultaneously empower coherent energy transfer in two different plasmon-exciton coupling subsystems. Relevant experimental [37, 38] and theoretical work [39] emerged as the extension of two-mode strong coupling. Cuadra et al. have successfully demonstrated three intermixed plasmon-exciton-trion coherent states at the single nanoparticle level under cryogenic conditions, which consist of an individual silver nanoantenna and monolayer WS<sub>2</sub> hybrid system [26]. Recently, Lan et al. realized active tuning of strong plasmon-exciton-trion coupling in Si/WS<sub>2</sub>/Au nanocavities by increasing the laser power [40]. In another work, Zhou et al. [41] demonstrated plasmon-assisted coherent energy transfer between far-detuned QEs, setting the foundation for future quantum networks.

Inspired by these pioneering works, in this study, we demonstrate strong interactions among plasmons in an individual Au@Ag nanocavity, Frenkel excitons in TDBC J-aggregates, and Wannier excitons in monolayer WS<sub>2</sub>. Three hybrid states formed by the biexcitons-plasmon coupling and double Rabi splitting phenomenon (137 meV and 124 meV) were observed under ambient conditions.

Furthermore, we reveal the mode competition between two coupled excitonic modes and optimize the multimode coupling nanosystems by controlling the coated J-aggregates spacers. Theoretical calculations indicate that the cavity morphology and environment temperature can tailor the degree of biexcitons-plasmon coupling. Modification in the dielectric constant of the WS<sub>2</sub> monolayer induced by tuning the temperature has also been extracted, which can well explain the temperature-resolved scattering spectra.

# 2 Results and discussion

## 2.1 Introducing biexcitons-plasmon coupling in a Au@Ag/J-aggregates/WS<sub>2</sub> nanocavity

As depicted in Figure 1a, the coupled system in this work is composed of Au@Ag core-shell nanocavity coating with TDBC J-aggregates, which is positioned on the surface of monolayer WS2. As an essential component, plasmonic nanocavity plays a critical role in providing a highlyenhanced local electric field, empowering different strong coupling channels with heterogeneous QEs. Frenkel-type excitons are formed in molecular materials, typically with small exciton radii and asymmetric charge distribution [42]. Therefore, they exhibit strong polar chemical properties. However, due to their formation inside molecules and weak interactions between electrons and holes, Frenkel-type excitons have short lifetimes, and it is challenging to achieve

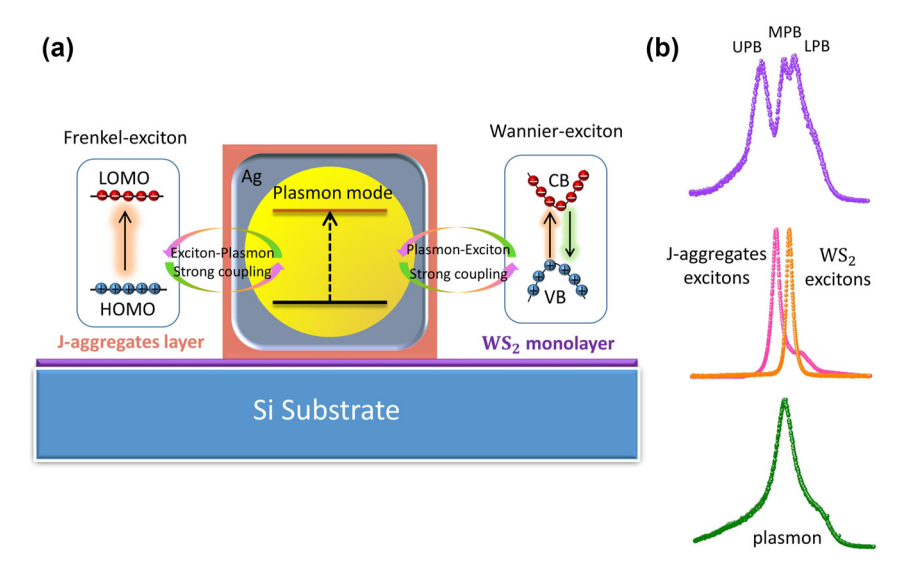


Figure 1: Concept of biexcitons-plasmon strong coupling between detuned excitonic materials and an individual metallic nanocavity. (a) Schematic showing a delicately designed QEs-nanoantenna structure which empowers simultaneous energy exchange with both Frenkel-excitons and Wannier-excitons. Ultimately, the newly formed biexcitons-plasmon hybrid states can possess the characteristics of both QEs. (b) Measured spectra of uncoupled components (lower) and multi-mode strong coupled nanosystem (upper) exhibit a distinct double Rabi-splitting signature.

long-lifetime luminescence. In contrast, Wannier-type excitons formed in crystals typically have longer lifetimes and larger exciton radii, along with lower charge transfer efficiency [43]. Here we take advantage of multimode coupling among plasmon, Frenkel-type excitons, and Wannier-type excitons, which enable the possibility to exhibit the best features of different excitonic materials (see Figure 1a). The electromagnetic coupling between the localized plasmon resonance and J-aggregates/WS2 excitons is different due to their spatial distribution variations. The excitons in Jaggregates are of Frenkel type, which is characterized by its strong binding energy (order of 1 eV), large dipole moment (0.7 e nm), and small Bohr radius (1 nm) [44]. Ultrathin Jaggregates monolayer is used to realize single-exciton level strong coupling [19]. It is demonstrated that only the Jaggregate exciton within the sufficient localized E-field can be involved in the strong coupling process. In our system, strong electromagnetic coupling between J-aggregates excitons and plasmon modes mainly happens at the sharp corners of Au@Ag nanorods. On the other hand, excitons in WS2 are of Wannier type, which is delocalized over several unit cells and possess larger scattering cross sections. Monolayer WS2 is a direct bandgap semiconductor, leading to excitons with enormous binding energies (700 meV) [45]. Moreover, the optical property of single-crystalline WS<sub>2</sub> is uniform across the entire two-dimensional flake, which is beneficial to form robust pl-exciton systems. To realize biexcitons-plasmon coupling, the spectra properties of the three uncoupled components are carefully investigated before sample assembling (as shown in Figure 1b). The PL spectra measured for the monolayer WS<sub>2</sub> (under ambient condition) shows a resonance peak at  $E_x = 2029$  meV, while the measured absorption resonance for the J-aggregates is  $E_i = 2099$  meV. The dark-field scattering spectrum of a typical Au@Ag nanocavity shows a broad resonance ( $E_{nl}$  = 2075 meV) in the middle of the two excitonic materials. The decay rate of the WS<sub>2</sub> excitons is  $\gamma_x = 26$  meV (measured by absorption spectrum in Figure S4) or 19 meV (measured by photoluminescence spectrum in Figure 1b). It is noteworthy that the extracted decay rate of J-aggregates ( $\gamma_i$  = 25 meV) and WS<sub>2</sub> is relatively small compared to the plasmon nanocavity ( $\gamma_{pl} = 144$  meV). When two adjacent excitonic modes spectral overlap with the plasmonic nanocavity, it might be possible to form a multi-mode coupling system. The top of Figure 1b shows the scattering spectra (solid purple curves) measured for the WS<sub>2</sub>/J-aggregates/Au@Ag nanocavity irradiated using a halogen lamp. Three new energy branches will be formed if excitons of both the Jaggregates and WS<sub>2</sub> interact intensively with the plasmonic mode, which is marked as the upper polariton branch (UPB),

the middle polariton branch (MPB), and the lower polariton branch (LPB).

## 2.2 The properties of plasmon-exciton subsystems

Before diving into the complex coupling among nanocavity, J-aggregates and WS2, we first investigate the properties of the two plexcitonic sub-systems. By controlling the Ag shell's thickness in the growth process, the localized surface plasmon resonance of Au@Ag nanocavity was carefully tuned from 651 nm to 565 nm, which crosses the exciton resonance of both J-aggregates and WS2. The fine-tuning originates from the high sensitivity of LSPR mode to the aspect ratio [19]. In Figure 2, the scattering spectrum of the nanocavity/J-aggregates hybrid shows two peaks and a dip at 592 nm, which is the exciton resonance of J-aggregates. To attain the dispersion curve, the scattering spectra of nanocavity/J-aggregates hybrid with different Ag shell thicknesses were measured. As shown in Figure 2c, the newly formed hybrid states' eigenenergies were extracted, exhibiting a distinct anticrossing phenomenon. A large Rabi splitting (~162 meV) was observed at resonant conditions. Compared to the plasmon and exciton linewidths ( $\gamma_{pl} = 150$  meV,  $\gamma_j = 25$  meV), the Rabi splitting energy  $\Omega_{pj} > \frac{\gamma_{pl} + \gamma_j}{2}$ , which indicates the nanocavity/I-aggregates hybrid has entered the strong coupling regime. Next, we investigate the strong coupling between plasmon and the WS2 excitons. The WS2 monolayers synthesized by chemical vapor deposition were transferred to Si/SiO<sub>2</sub> substrates with a 100 nm thick SiO<sub>2</sub> film. In Figure 2d, the dark-field image of the wafer was demonstrated, showing a firm and direct contact between nanocavities and WS2 monolayers. Two new eigenstates were formed at the flanks of the WS2 excitonic resonance  $(\lambda_x = 612 \text{ nm})$ , as shown in Figure 2e. In Figure 2f, the energy dispersion of the upper polariton branches (UPB) and the lower polariton branches (LPB) exhibit anticrossing behavior. A Rabi splitting of 110 meV is observed, which close to satisfy the criteria for strong coupling ( $\Omega_{px} > \frac{\gamma_{pl} + \gamma_x}{2}$ ).

## 2.3 Mode competition within the localized plasmonic hotspots

The strong interaction with nanocavity required sufficient electric field enhancement. The mode volume of Au@Ag nanocavity is extremely small (~240 nm<sup>3</sup>), leading to inevitable mode competition between two excitonic materials within the plasmonic hotspots. Thus, we can trigger and manipulate the biexcitons-plasmon strong coupling by optimizing the interaction distance. For the

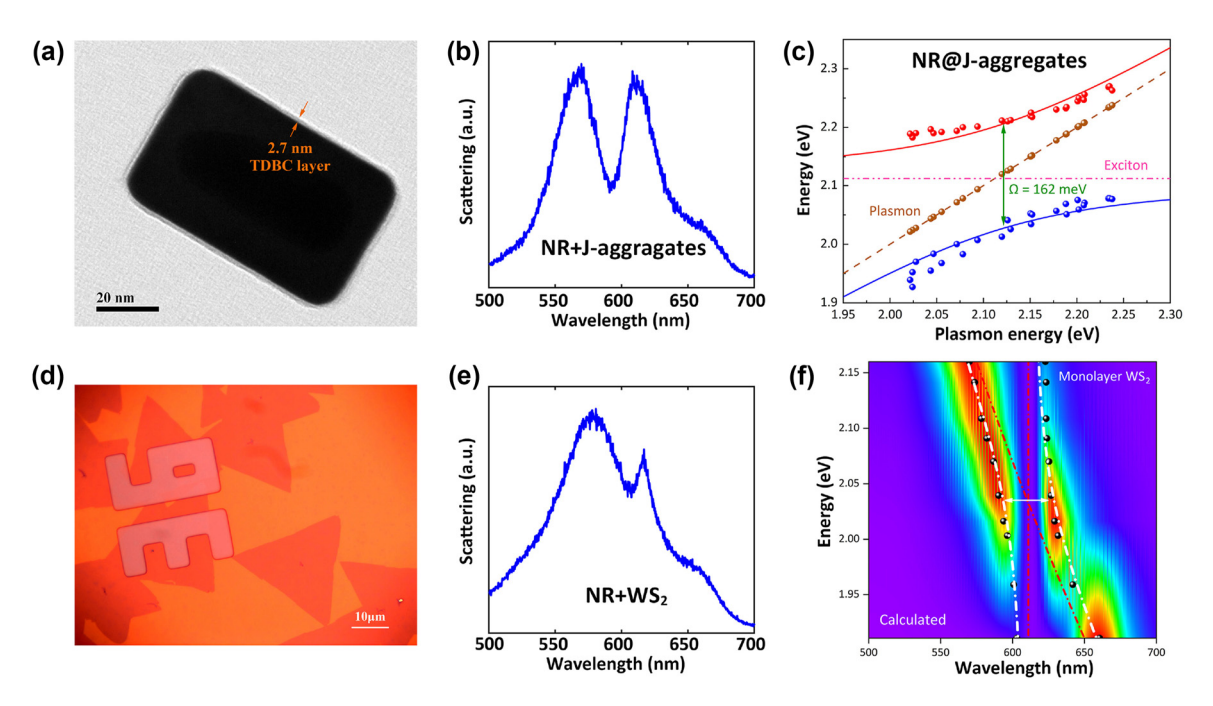


**Figure 2:** Single-mode plasmon-exciton strong coupling. (a) High-resolution TEM image of Au@Ag nanorod coated with 2.7 nm TDBC J-aggregates layers. (b) Scattering spectra of resonate Au@Ag nanorod and J-aggregates hybrid nanosystem. (c) Dispersion of plexciton with UPB and LPB varied as a function of plasmon energy, presenting a Rabi splitting up to 162 meV. (d) Bright-field image of WS $_2$  monolayer collected by a 100× objective. (e) Scattering spectra of red-detuned Au@Ag nanorod and monolayer WS $_2$  nanosystem. (f) Calculated dispersion of single Au@Ag nanocavity and WS $_2$  strong coupled system, presenting a Rabi splitting of 110 meV.

I-aggregates/Au@Ag nanocavity shown in Figure 3a, the scattering dip appears at ~592 nm. The Rabi splitting of the nanocavity/dye hybrid system becomes more significant as the J-aggregates layers grow. The corresponding plasmonic cavity E-field distributions in the xz planes are shown in Figure 3b. It indicates that more J-aggregates excitons participate in the coupling process as the dye molecular layers become thicker, which leads to larger Rabi splitting in Figure 3a. On the other hand, the dye molecular layers also serve as the spacer layer in the nanocavity/J-aggregates/WS<sub>2</sub> hybrid system, which significantly impairs the coupling strength between nanocavity and WS<sub>2</sub>. As shown in upper Figure 3c, when the dye molecular layers are rather thin (d = 1 nm), the coupling strength between nanocavity and J-aggregates is weak, and the MPB leans towards  $\lambda_I$ . In lower Figure 3c, when the dye molecular layers are thick (d = 15 nm), the interaction between WS<sub>2</sub> and nanocavity is almost blocked. The mode competition is well reflected in the MPB resonance. The pink/orange dashed line indicates the location of J-aggregates/WS<sub>2</sub> excitons resonance. As the J-aggregates layers become thicker, the WS<sub>2</sub> excitons in the plasmonic hotspots decrease. Interestingly, the MPB resonance is pushed toward WS2 resonance as the J-aggregates dominate the hybrid system. On the contrary, the MPB resonance would lean toward J-aggregates resonance when WS2

is dominant. We found that MPB would locate at the center of J-aggregates/WS $_2$  resonance when the coating thickness of J-aggregates is  $\sim 3$  nm. This particular coating thickness ensures both J-aggregates and WS $_2$  excitons can actively participate in the strong coupling process, which guides our subsequent experiments.

# 2.4 Biexcitons-plasmon coupling in Au@Agnanocavity/J-aggregates/WS<sub>2</sub> hybrids

To construct a plasmon-biexcitons strong coupling nanosystems, we first coat a uniform J-aggregates layer ( $\sim$ 3 nm) on the surface of the Au@Ag nanocavities, then the hybrids were facially integrated with a WS $_2$  monolayer. Here the J-aggregates layers were also used as a dielectric spacer layer, significantly impacting the plasmon-WS $_2$  coupling strength. We use a correlative dark-field and SEM imaging method to obtain the morphology and spectroscopic information of individual nanocavity/J-aggregates/WS $_2$  hybrids. As illustrated in Figure 1a, when both the J-aggregates and WS $_2$  monolayer were within the plasmon E-field hotspots, coherent energy transfer between plasmon and biexcitons occurred due to the field enhancement effect of plasmon mode. Consequently, new hybrid polariton states would be

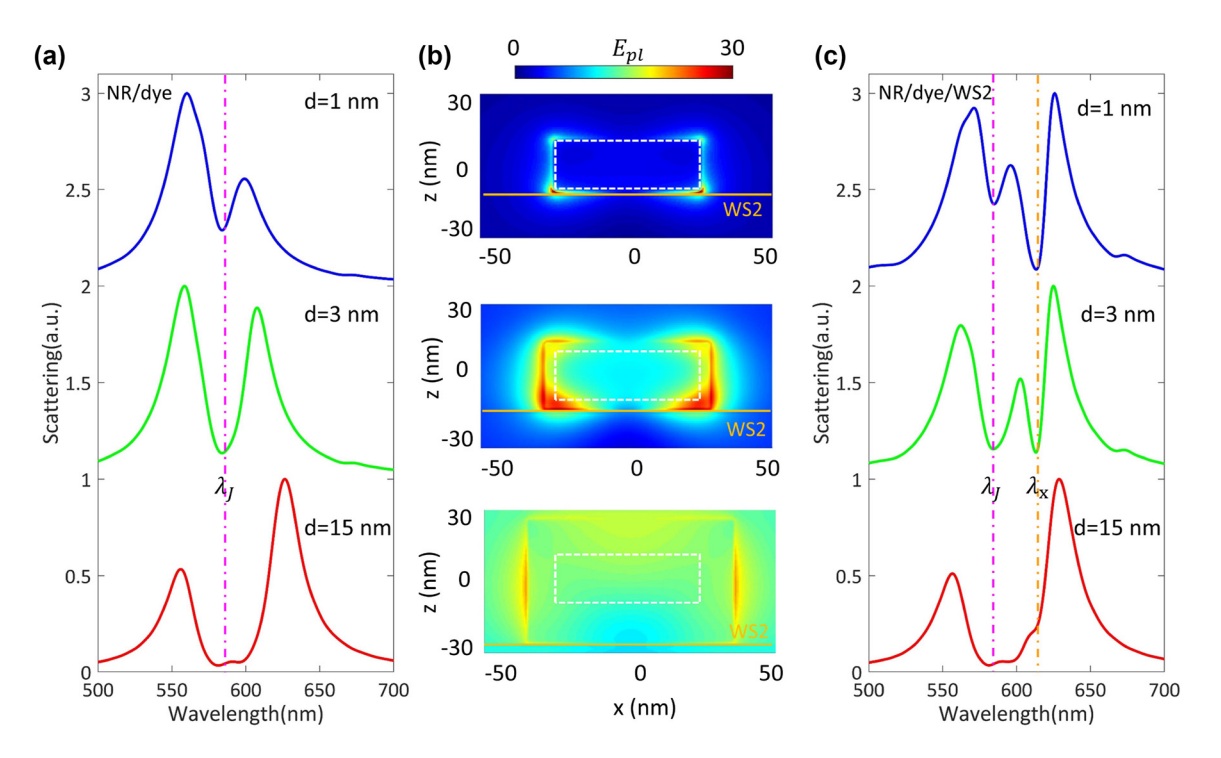


**Figure 3:** Analysis of mode competition for  $WS_2/dye/Au@Ag$  nanocavity coupled systems. (a) Scattering spectra calculated for Au@Ag nanocavity coated with different J-aggregate thicknesses. (b) The plasmonic cavity E-field distributions calculated at 592/602/612 nm. The white dashed lines indicate the outline of the Au@Ag nanorod. The solid orange lines indicate the position of the  $WS_2$  monolayer. (c) Corresponding scattering spectra calculated for  $WS_2/dye/Au@Ag$  nanocavity with different J-aggregate thicknesses.

produced, as shown in Figure 1b, which is more complicated than traditional two-mode coupled nanosystems. We measured more than 200 dark-field scattering spectra of different nanocavity/J-aggregates/WS<sub>2</sub> hybrids, where the plasmon resonance was tuned by adjusting the thickness of Ag shells during the synthesis process. Figure 4a shows the scattering spectra of five representative nanocavity/Jaggregates/WS2 hybrids, demonstrating the spectral evolution of plasmon-biexcitons coupling in different detuned conditions. Three scattering peaks appear at the flank of the J-aggregates/WS<sub>2</sub> excitons resonance, corresponding to the three eigenenergies of the plasmon-biexcitons coupling systems. In Figure 4a, as the Ag shell becomes thicker, the aspect ratio of Au@Ag nanocavities increased. The plasmon resonance was tuned to blue-shift, leading to a synchronized blue-shift in all three eigenenergies, while the relative intensity of three scattering peaks would also variate. Meanwhile, the two dips of scattering spectra remain unchanged, corresponding to the exciton resonance of the J-aggregates/WS<sub>2</sub> monolayer. It provides strong evidence that the new hybrid polariton states result from plasmon/Jaggregates/WS2 interaction. For the plasmon-biexcitons coupling in our experiment, the eigenmodes' energy can be described using the three-coupled oscillator model (TCOM),

which is written as [46-49].

$$\begin{pmatrix}
E_{pl} - i\frac{\gamma_{pl}}{2} & g_j & g_x \\
g_j & E_j - i\frac{\gamma_j}{2} & 0 \\
g_x & 0 & E_x - i\frac{\gamma_x}{2}
\end{pmatrix}
\begin{pmatrix}
\alpha \\
\beta \\
\gamma
\end{pmatrix} = E
\begin{pmatrix}
\alpha \\
\beta \\
\gamma
\end{pmatrix} (1)$$

where  $E_{nl}$ ,  $E_0$ , and  $E_x$  are the energies for cavity plasmon resonance, J-aggregates exciton resonance and WS2 exciton resonance, respectively. Here,  $\gamma_{pl}$ ,  $\gamma_0$ , and  $\gamma_x$  represent the corresponding dissipation rates, and  $g_i/g_x$  reflects the plasmon-J excitons/plasmon-WS2 excitons coupling strength. Notably, the J-aggregates/WS2 coupled strength is negligible due to the detuning between two excitons. E is the hybrid polariton energies of the three-mode coupling system.  $\alpha$ ,  $\beta$ , and  $\gamma$  are the Hopfield coefficients.  $|\alpha|^2$ ,  $|\beta|^2$ , and  $|\gamma|^2$  indicate the proportion of plasmon, J-aggregates and WS<sub>2</sub> excitons in the hybrid polariton states, which satisfy  $|\alpha|^2 + |\beta|^2 + |\gamma|^2 = 1$ . By solving the characteristic equation (1), three unique solutions  $E_{II}, E_{M}, E_{L}$ can be obtained for E. In Figure 4b, the theoretical fitting results are shown by three solid curves, which represent the hybrid states of three anti-crossed bands, corresponding to the upper polariton branch (UPB), middle polariton branch

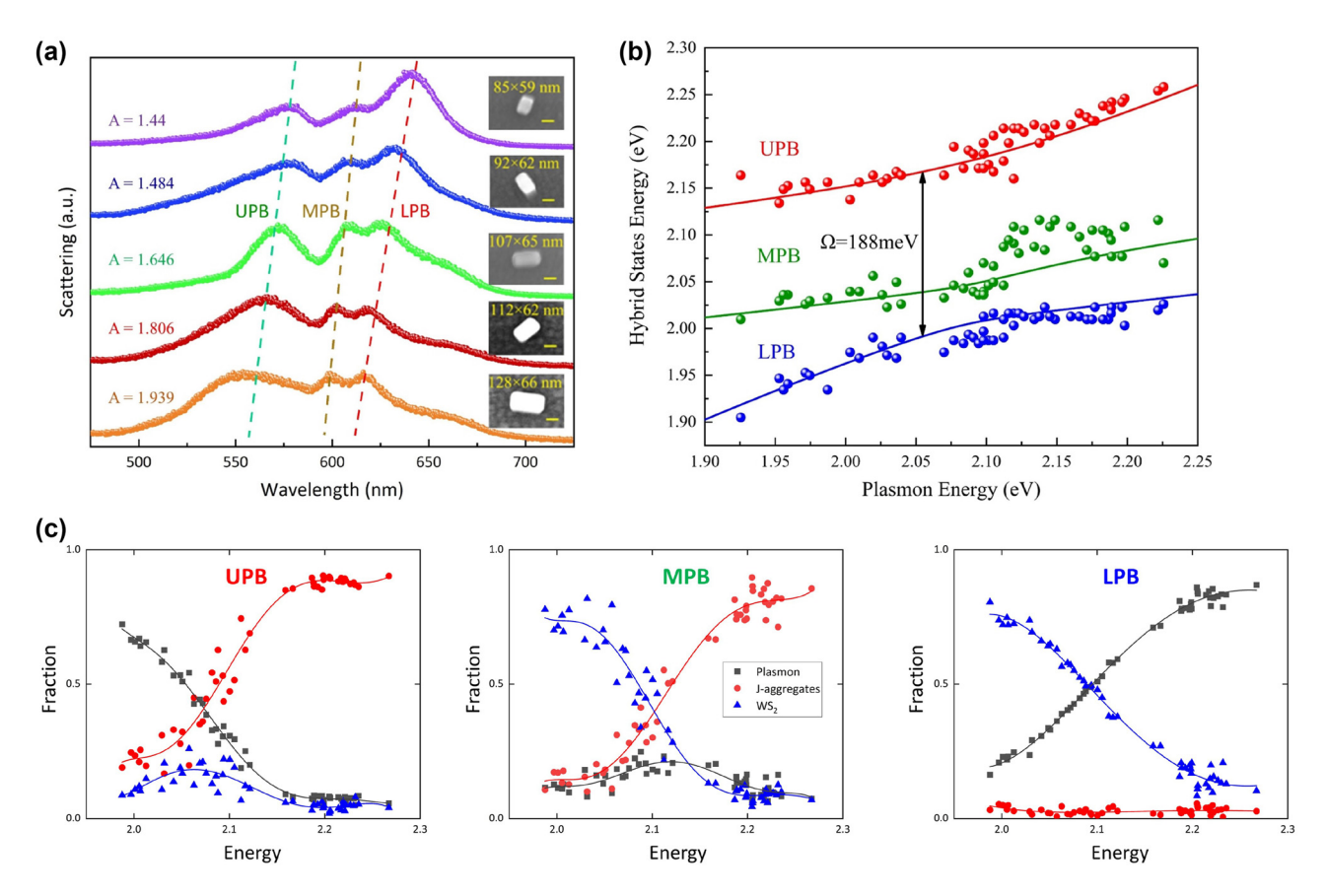


**Figure 4:** Manipulating the biextions-plasmon coupling with a structure tuning method. (a) Scattering spectra of different plasmon-biexciton strong coupling systems constructed by using Au@Ag nanocavities with different aspect ratios. The SEM and corresponding CCD images of the measured WS<sub>2</sub>/J-aggregates/Au@Ag nanocavities are shown in the insets. (b) Dispersion of the eigenenergies of the three coherent hybrid states. The red/green/blue curves represent the theoretical values for UPB/MPB/LPB, while the colored symbols represent the scattering peaks obtained from the experimental data. (c) Hop-field coefficients for plasmon, J-aggregates exciton, and WS<sub>2</sub> exciton contributions to UPB, MPB, and LPB states as a function of the plasmon energy.

(MPB) and lower polariton states (LPB). The resonance energy of plasmon nanocavity  $E_{nl}$  is essential for analyzing anti-crossing behavior in strong coupling systems. However, it can not be directly obtained by experimental measurements because the resonance of plasmonic nanocavities would red-shift after coating with molecule layers. To perform the anti-crossing analysis, we first obtain the corresponding energy for the upper  $(E_U)$ , middle  $(E_M)$ , and lower  $(E_L)$  polariton branches from dark-field scattering spectra. Then the exciton resonance of J-aggregate  $(E_i)$  and WS<sub>2</sub>  $(E_x)$ is extracted from the absorption measurements. Finally, we obtain the unknown value of  $E_{pl}$  using energy conservation equality:  $E_{nl} + E_i + E_x = E_U + E_M + E_L$ . The equality originates from trace invariance of the matrix representation of the Hamiltonian, which was proposed in recent research [26, 50] to analyze three-mode coupling systems.

As shown in Figure 4b, the TCOM fits well with our experimental results, indicating a giant Rabi splitting energy of 188 meV at the center of J-aggregates/WS $_2$ 

excitonic resonances. It is worth noting that the fitting results in the coupling strengths are  $g_i = 68.7 \text{ meV}$  and  $g_x = 62.1$  meV, respectively. Therefore, when the plasmon mode is resonant with J-aggragates/WS2 excitons, the splittings extracted at zero detuning are  $\Omega_I = 137 \text{ meV}(E_{pl} =$  $E_i$ ) and  $\Omega_X=124~{\rm meV}(E_{pl}=E_X)$ . The coupling strengths are slightly decreased compared to the plasmon-single exciton coupling situation but still satisfy the strong coupling criterion of  $g_i > |y_{pl} - y_j|/4 = 31.25 \text{ meV}$  and  $g_x > |y_{pl} - y_j|/4 = 31.25 \text{ meV}$  $y_x|/4 = 32.75$  meV. Figure 4c shows the calculated Hopfield coefficients, which indicate the proportion of plasmon/Jaggregates/WS2 energy in each hybrid polariton state. Specifically, the coupling between J-aggregates and plasmon dominates the UPB, while the coupling between WS2 and plasmon dominates the LPB. It results from the detuning between plasmon and J-aggregates/WS2 excitons. The coupling strength grows as the detuning decrease. The properties of MPB are more complicated, which contains few proportions of plasmon compared to its excitonic parts. Therefore in Figure 4b MPB shows less disperse than UPB/LPB. Also, since  $E_I > E_X$ , J-aggregates excitons show more impact in MPB regarding the high energy regime. The strong coupling criterion for three elementary excitations can be expressed as  $\Omega > \alpha_1 \kappa_{upb} + \alpha_2 \kappa_{mpb} + \alpha_3 \kappa_{lpb}$  [36, 40].

Here,  $\alpha_1, \alpha_2$ , and  $\alpha_3$  represent the fractions of the UPB/MPB/LPB in the hybrid polariton states;  $\kappa_{upb}, \kappa_{mpb},$  and  $\kappa_{upb}$  denote the linewidths of the UPB/MPB/LPB. By extracting the zero-detuned data from Figure 4c, the linewidths of each branch can be expressed as follows:

$$\begin{cases} \kappa_{upb} = 52.6 \% \gamma_{pl} + 40.7 \% \gamma_j + 6.7 \% \gamma_x \\ \kappa_{mpb} = 22.1 \% \gamma_{pl} + 40.9 \% \gamma_j + 37 \% \gamma_x \\ \kappa_{lpb} = 36.7 \% \gamma_{pl} + 7 \% \gamma_j + 56.3 \% \gamma_x \end{cases}$$
(2)

The following formula can derive the weight coefficients of UPB/MPB/LPB [31]:

$$\begin{cases} \alpha_1 = \frac{\kappa_{upb}}{\kappa_{upb} + \kappa_{mpb} + \kappa_{lpb}} \\ \alpha_2 = \frac{\kappa_{mpb}}{\kappa_{upb} + \kappa_{mpb} + \kappa_{lpb}} \\ \alpha_3 = \frac{\kappa_{lpb}}{\kappa_{upb} + \kappa_{mpb} + \kappa_{lpb}} \end{cases}$$
(3)

By substituting Equations (2) and (3), we can derive the criterion for the strong coupling of plasmon/Jaggregates/WS<sub>2</sub> as  $\Omega > \alpha_1 \cdot \kappa_{upb} + \alpha_2 \cdot \kappa_{mpb} + \alpha_3 \cdot \kappa_{lpb} =$ 74.8 meV. In our case, we measured a relatively large Rabi splitting  $\Omega \approx$  188 meV at zero-detuned point (as shown in Figure 4b), which satisfy the strong coupling criterion. The  $\operatorname{detuning} \Omega > \alpha_1 \cdot \kappa_{upb} + \alpha_2 \cdot \kappa_{mpb} + \alpha_3 \cdot \kappa_{lpb}.$ 

# 2.5 Adjusting the excitonic resonance of a WS<sub>2</sub> monolayer by temperature control and fine-tuning the biexcitons-plasmon

Finally, in Figure 5, we demonstrate that the biexcitonsplasmon strong coupling nanosystem can be actively and reversibly manipulated by tuning the environment temperature. WS2 monolayer possesses multidimensional adjustable optical properties, for example, its band gap varies with environmental temperature. Figure 5b indicates that the real and imaginary parts of a WS2 monolayer would regularly red-shift to a longer wavelength with increasing environmental temperature, which offers us the opportunity to manipulate the biexcitons-plasmon coupling strength. The WS2 excitonic energy under different temperatures can be theoretically described by O'Donnell Model [51, 52]. In Figure S3, we calculate the WS<sub>2</sub> exciton resonance in the 200 K-400 K range using O'Donnell model, which indicates a red-shift from 606 nm to 624 nm. In Figure 5a, we show the scattering spectra of Au@Ag nanocavity/Jaggregates/WS2 calculated in different temperatures, which indicates that the middle and lower biexcitons-plasmon hybrid states could be accurately adjusted via temperature control. Here, the aspect ratio of the simulated nanoparticle is set as 1.65 and the plasmon resonance of the nanocavity is 592 nm, which overlay with the J-aggregates' excitonic

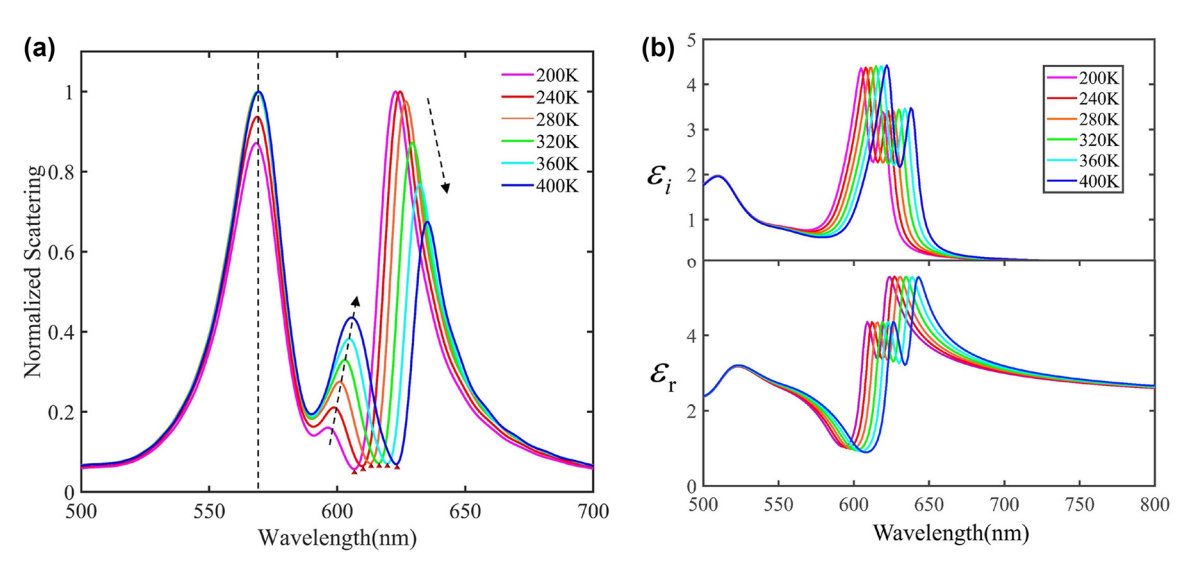


Figure 5: Fine-tuning the biextions-plasmon coupling by temperature control. (a) Normalized scattering spectra calculated for WS<sub>2</sub>/J-aggregates/Au@Ag nanocavities in different temperatures. (b) Complex dielectric constants of a WS<sub>2</sub> monolayer in different temperature conditions.

energy. The thickness of the coating J-aggregates is set as 3 nm and then facially integrated with monolayer WS<sub>2</sub>. The dashed arrows in Figure 5a shows that the UPB rarely change during the regulation process, while MPB and LPB gradually redshift as the temperature increase. As a result, the Rabi splitting between UPB and MPB increases from 191 meV to 226 meV. Notably, the scattering dips between MPB and LPB (marked with red triangles in Figure 5a) are in accordance with the calculated WS<sub>2</sub> exciton resonance. The tuning accuracy of MPB/LPB resonance wavelength can reach up to ~1 nm when the variation of temperature is ~10 K, which provides a delicate and reversible method to control the biexcitons-plasmon coupling system.

### 3 Conclusions

In summary, we have systematically investigated the spectral properties and manipulating methods of plasmonbiexcitons strong coupling in Au@Ag/J-aggregates/WS<sub>2</sub> hybrid nanosystems. Three new plexciton branches formed by multimode hybridization are observed from the darkfield scattering spectra, which present a giant exciton-plasmon-exciton energy splitting ~188 meV at the center of excitonic resonances. Hopfield coefficient calculations reveal the plasmon-biexcitons have properties that are intermediate between plasmons and J-aggregates/WS2 excitons, which enable the possibility to obtain the best features of both metal and semiconductors. Furthermore, we have investigated the mode competition between heterogeneous excitonic materials and proposed the optimal parameters for J-aggregates spacer, which is in the middle range of localized plasmonic hotspots. Accordingly, from the WS<sub>2</sub> exciton perspective, we have also demonstrated the dynamic control of plasmon-biexcitons via thermal regulation. The temperature-resolved spectra are ascribed to the dielectric constant modification of WS<sub>2</sub>, which significantly affect the coupling strength between plasmon and  $X_A$  excitons. Our findings offer a versatile platform to construct and manipulate multiqubit coupling in room-temperature conditions and pave the way for developing diverse plexcitonic devices.

### 4 Methods

### 4.1 Sample preparation

We fabricated the cuboidal Au@Ag nanocavity with sharp edges using a seed-mediated growth method (details are provided in Supporting Information, Section 1). Figure S1 shows the high-resolution TEM image of one typical Au@Ag nanocavities with proper dimensions (diameter  $\sim$ 48.2  $\pm$  1.4 nm and length  $\sim$ 78.3  $\pm$  3.1 nm). To boost the plasmon-exciton coupling strength, the curvature radius of the Ag shell at the edgy is tailored to  $\sim\!2\,\mathrm{nm}$ , causing a dramatic small mode volume down to a few hundred cubic nanometers (see Supporting Information, Figure S2). J-aggregates layers were firmly attached to the surface of Au@Ag nanocavity via electrostatic interaction, which forms a typical plasmon-exciton strong coupling system. The nanocavity/J-aggregates hybrid was then transferred to a bare silicon wafer substrate for subsequent measurements.

#### 4.2 Optical measurements

We use a reflection-type dark-field scattering experiment setup to investigate the optical properties of the individual nanocavity. Individual Au@Ag nanocavities were optically characterized using an upright microscope (BX51, Olympus) combined with an imaging spectrograph (IsoPlane 160, Princeton Instrument) and an EMCCD camera (Ultra 888, Andor). The sample surface was illuminated with broadband white light from a Laser-Driven Light Source (EO-99X, Energetig), which was focused onto the sample surface using a 100X dark-field condenser (NA = 0.4). In addition, numerical symbols in the silicon wafer were used to locate individual nanocavity in dark-filed and SEM imaging.

Acknowledgment: The authors acknowledge Dr. J. Q. Guo's assistance with the sample synthesis and Prof. Z. K. Zhou and Prof. R. M. Liu for helping with the optical measurements discussion.

**Author contributions:** All authors have accepted responsibility for the entire content of this manuscript and approved its submission.

**Research funding:** This work is supported by the National Natural Science Foundation of China (12204061,12174037) and the State Key Laboratory of Information Photonics and Optical Communications (No. IPOC2021ZZ02).

Conflict of interest statement: Authors state no conflicts of interest.

**Data availability:** The data that support the findings of this study are available from the corresponding author upon reasonable request.

### References

- [1] P. Törmä and W. L. Barnes, "Strong coupling between surface plasmon polaritons and emitters: a review," Rep. Prog. Phys., vol. 78, no. 1, pp. 013901 - 013935, 2014.
- [2] K. Santhosh, O. Bitton, L. Chuntonov, and G. Haran, "Vacuum Rabi splitting in a plasmonic cavity at the single quantum emitter limit," Nat. Commun., vol. 7, no. 1, 2016, Art. no. ncomms11823.
- [3] H. Deng, G. Weihs, C. Santori, J. Bloch, and Y. Yamamoto, "Condensation of semiconductor microcavity exciton polaritons," Science, vol. 298, no. 5591, pp. 199-202, 2002.
- [4] S. R. K. Rodriguez, J. Feist, M. A. Verschuuren, F. J. Garcia Vidal, and J. Gómez Rivas, "Thermalization and cooling of plasmon-exciton polaritons: towards quantum condensation," Phys. Rev. Lett., vol. 111, no. 16, pp. 166802-166807, 2013.

- [5] J. T. Zhang, Y. Tang, K. Lee, Kwan, and M. Ouyang, "Tailoring light-matter-spin interactions in colloidal heteronanostructures," Nature, vol. 466, no. 7302, pp. 91-95, 2010.
- [6] P. Vasa, W. Wang, R. Pomraenke, et al., "Optical Stark effects in J-aggregate – metal hybrid nanostructures exhibiting a strong exciton - surface-plasmon-polariton interaction," Phys. Rev. Lett., vol. 114, no. 3, p. 036802, 2015.
- [7] R. Sáez-Blázguez, J. Feist, A. I. Fernández-Domínguez, and F. J. García-Vidal, "Enhancing photon correlations through plasmonic strong coupling," Optica, vol. 4, no. 11, pp. 1363-1367, 2017.
- [8] M. Hensen, T. Heilpern, S. K. Gray, and W. Pfeiffer, "Strong coupling and entanglement of quantum emitters embedded in a nanoantenna-enhanced plasmonic cavity," ACS Photonics, vol. 5, no. 1, pp. 240-248, 2018.
- [9] D. Pan, H. Wei, Z. L. Jia, and H. X. Xu, "Mode conversion of propagating surface plasmons in nanophotonic networks induced by structural symmetry breaking," Sci. Rep., vol. 4, no. 1, pp. 4993-4999, 2014.
- [10] S. Johnson, P. R. Dolan, and J. M. Smith, "Diamond photonics for distributed quantum networks," Prog. Quantum Electron., vol. 55, no. 11, pp. 129-165, 2017.
- [11] H. Y. Shan, Z. X. Liu, X. L. Wang, et al., "Spontaneous emission of plasmon-exciton polaritons revealed by ultrafast nonradiative decays," Laser Photonics Rev., vol. 14, no. 12, p. 2000233, 2020.
- [12] H. Wei, X. H. Yan, Y. J. Niu, Q. Li, Z. Jia, and H. Xu, "Plasmon – exciton interactions: spontaneous emission and strong coupling," Adv. Funct. Mater., vol. 31, no. 51, p. 2100889,
- [13] L. Y. Zhao, Q. Y. Shang, M. L. Li, Y. Liang, C. Li, and Q. Zhang, "Strong exciton-photon interaction and lasing of two-dimensional transition metal dichalcogenide semiconductors," Nano Res., vol. 14, no. 6, pp. 1937-1954, 2021.
- [14] J. B. You, X. Xiong, P. Bai, et al., "Reconfigurable photon sources based on quantum plexcitonic systems," Nano Lett., vol. 20, no. 6, pp. 4645-4652, 2020.
- [15] T. Volz, A. Reinhard, M. Winger, et al., "Ultrafast all-optical switching by single photons," Nat. Photonics, vol. 6, no. 9, pp. 605-609, 2012.
- [16] G. Lerario, A. Fieramosca, F. Barachati, et al., "Room-temperature superfluidity in a polariton condensate," Nat. Phys., vol. 13, no. 9, pp. 837 – 841, 2017.
- [17] N. Kongsuwan, X. Xiong, P. Bai, et al., "Quantum plasmonic immunoassay sensing," Nano Lett., vol. 19, no. 9, pp. 5853-5861,
- [18] W. Du, T. Wang, H. S. Chu, and C. A. Nijhuis, "Highly efficient on-chip direct electronic – plasmonic transducers," Nat. Photonics, vol. 11, no. 10, pp. 623-627, 2017.
- [19] R. M. Liu, Z. K. Zhou, Y. C. Yu, et al., "Strong light-matter interactions in single open plasmonic nanocavities at the quantum optics limit," Phys. Rev. Lett., vol. 118, no. 23, p. 237401, 2017.
- [20] F. Benz, M. K. Schmidt, A. Dreismann, et al., "Single-molecule optomechanics in "picocavities"," Science, vol. 354, no. 6313, pp. 726-729, 2016.
- [21] R. Chikkaraddy, B. De Nijs, F. Benz, et al., "Single-molecule strong coupling at room temperature in plasmonic nanocavities," Nature, vol. 535, no. 7610, pp. 127-130, 2016.
- [22] G. Heiko, J. M. Hamm, T. Tufarelli, O. Hess, and B. Hecht, "Near-field strong coupling of single quantum dots," Sci. Adv., vol. 4, no. 3, p. eaar4906, 2018.

- [23] L. Liu, Y. M. Landobasa, T. T. Wu, et al., "Plasmon-induced thermal tuning of few-exciton strong coupling in 2D atomic crystals," Optica, vol. 8, no. 11, pp. 1416-1423, 2021.
- [24] J. Y. Li, W. Li, J. Liu, et al., "Room-temperature strong coupling between a single quantum dot and a single plasmonic nanoparticle," Nano Lett., vol. 22, no. 12, pp. 4686-4693, 2022.
- [25] J. X. Wen, H. Wang, W. L. Wang, et al., "Room-temperature strong light—matter interaction with active control in single plasmonic nanorod coupled with two-dimensional atomic crystals," Nano Lett., vol. 17, no. 8, pp. 4689-4697, 2017.
- [26] J. Cuadra, D. G. Baranov, M. Wersall, R. Verre, T. J. Antosiewicz, and T. Shegai, "Observation of tunable charged exciton polaritons in hybrid monolayer WS2- plasmonic nanoantenna system," Nano Lett., vol. 18, no. 3, pp. 1777 – 1785, 2018.
- [27] D. Zheng, S. P. Zhang, Q. Deng, M. Kang, P. Nordlander, and H. Xu, "Manipulating coherent plasmon—exciton interaction in a single silver nanorod on monolayer WSe2," Nano Lett., vol. 17, no. 6, pp. 3809 - 3814, 2017.
- [28] J. X. Wen, H. Wang, H. J. Chen, S. Deng, and N. Xu, "Room-temperature strong coupling between dipolar plasmon resonance in single gold nanorod and two-dimensional excitons in monolayer WSe2," Chin. Phys. B, vol. 27, no. 9, p. 096101, 2018.
- [29] H. Wang, H. Y. Wang, L. Wang, et al., "Multimode coherent hybrid states: ultrafast investigation of double Rabi splitting between surface plasmons and sulforhodamine 101 dyes," Adv. Opt. Mater., vol. 5, no. 8, p. 1600857, 2017.
- [30] A. H. Rose, J. R. Dunklin, H. Y. Zhang, et al., "Plasmon-Mediated coherent superposition of discrete excitons under strong exciton - plasmon coupling in few-layer MoS2 at room temperature," Adv. Opt. Mater., vol. 5, no. 8, p. 1600857, 2017.
- [31] B. W. Li, S. Zu, Z. P. Zhang, et al., "Large Rabi splitting obtained in Aq-WS2 strong-coupling heterostructure with optical microcavity at room temperature," Opto-Electron. Adv., vol. 2, no. 5, p. 190008,
- [32] D. M. Coles, N. Somaschi, P. Michetti, et al., "Polariton-mediated energy transfer between organic dyes in a strongly coupled optical microcavity," Nat. Mater., vol. 13, no. 7, pp. 712-719, 2014.
- [33] A. V. Zasedatelev, A. V. Baranikov, D. Urbonas, et al., "A room-temperature organic polariton transistor," Nat. Photonics, vol. 13, no. 6, pp. 378-383, 2019.
- [34] D. Melnikau, A. A. Govyadinov, A. Sanchez-Iglesias, et al., "Double Rabi splitting in a strongly coupled system of core-shell Au@ Ag nanorods and J-aggregates of multiple fluorophores," J. Phys. Chem. Lett., vol. 10, no. 20, pp. 6137-6143, 2019.
- [35] Y. J. Niu, L. Gao, H. X. Xu, and H. Wei, "Strong coupling of multiple plasmon modes and excitons with excitation light controlled active tuning," Nanophotonics, vol. 12, no. 4, pp. 735-742, 2023.
- [36] S. M. Liu, F. Deng, W. J. Zhuang, et al., "Optical introduction and manipulation of plasmon – exciton – trion coupling in a Si/WS2/Au nanocavity," ACS Nano, vol. 16, no. 9, pp. 14390-14401, 2022.
- B. Munkhbat, D. G. Baranov, A. Bisht, et al., "Electrical control of hybrid monolayer tungsten disulfide – plasmonic nanoantenna light—matter states at cryogenic and room temperatures," ACS Nano, vol. 14, no. 1, pp. 1196-1206, 2020.
- [38] J. J. Ye, Y. T. Pan, G. H. Liu, et al., "Strong coupling between a plasmon mode and multiple different exciton states," Sci. China: Phys., Mech. Astron., vol. 66, no. 4, p. 244212, 2023.
- [39] P. Jiang, G. Song, Y. L. Wang, C. Li, and L. Yu, "Tunable strong exciton - plasmon - exciton coupling in

- WS2-J-aggregates-plasmonic nanocavity," Opt. Express, vol. 27, no. 12, pp. 16613-16623, 2019.
- [40] F. Deng, H. X. Huang, J. D. Chen, et al., "Greatly enhanced plasmon – exciton coupling in Si/WS2/Au nanocavities," Nano Lett., vol. 20, no. 1, pp. 220-228, 2021.
- [41] W. B. Zhang, J. B. You, J. F. Liu, et al., "Steering room-temperature plexcitonic strong coupling: a diexcitonic perspective," Nano Lett., vol. 21, no. 21, pp. 8979 – 8986, 2021.
- [42] S. M. Ivanov, S. D. Schulze, J. Polyutov, et al., "Exciton—vibrational coupling in the dynamics and spectroscopy of Frenkel excitons in molecular aggregates," Phys. Rep., vol. 567, pp. 1-78, 2015.
- [43] T. Christian, "Optical dispersion by Wannier excitons," Phys. Rev. Lett., vol. 75, no. 22, p. 4090, 1995.
- [44] L. C. Flatten, D. M. Coles, Z. Y. He, et al., "Electrically tunable organic—inorganic hybrid polaritons with monolayer WS2," Nat. Commun., vol. 8, no. 1, p. 14097, 2017.
- [45] B. R. Zhu, X. Chen, and X. D. Cui, "Exciton binding energy of monolayer WS2," Sci. Rep., vol. 5, no. 1, p. 9218, 2015.
- [46] D. G. Lidzey, D. D. Bradley, A. Armitage, S. Walker, and M. S. Skolnick, "Photon-mediated hybridization of Frenkel excitons in organic semiconductor microcavities," Science, vol. 288, no. 5471, pp. 1620-1623, 2000.
- [47] H. Yang, J. Yao, X. W. Wu, D. J. Wu, and X. J. Liu, "Strong plasmon - exciton - plasmon multimode couplings in threelayered

- Aq J-Aggregates Aq nanostructures," J. Phys. Chem. C, vol. 121, no. 45, pp. 25455 - 25462, 2017.
- [48] M. Pelton, S. D. Storm, H. X. Leng, et al., "Strong coupling of emitters to single plasmonic nanoparticles: exciton-induced transparency and Rabi splitting," Nanoscale, vol. 11, no. 31, pp. 14540-14552, 2019.
- [49] A. Khalil, A. A. Ibrahim, L. J. Huang, A. E. Miroshnichenko, and H. T. Hattori, "Boosting strong coupling in a hybrid WSe2 monolayer - anapole - plasmon system," ACS Photonics, vol. 8, no. 2, pp. 489-496, 2021.
- [50] X. B. Han, F. Li, Z. C. He, et al., "Double Rabi splitting in methylene blue dye-Ag nanocavity," Nanophotonics, vol. 11, no. 3, pp. 603 – 611, 2022.
- [51] K. P. O'donnell and X. chen, "Temperature dependence of semiconductor band gaps," Appl. Phys. Lett., vol. 58, no. 25, pp. 2924-2926, 1991.
- [52] T. W. Lo, Q. Zhang, M. Qiu, et al., "Thermal redistribution of exciton population in monolayer transition metal dichalcogenides probed with plasmon-exciton coupling spectroscopy," ACS Photonics, vol. 6, no. 2, pp. 411-421, 2019.

**Supplementary Material:** This article contains supplementary material (https://doi.org/10.1515/nanoph-2023-0304).